

Transmission gap, Bragg-like reflection, and Goos-Hänchen shifts near the Dirac point inside a negative-zero-positive index metamaterial slab

Xi Chen^{1,2*}, Li-Gang Wang^{3,4†}, and Chun-Fang Li^{1‡}

¹ *Department of Physics, Shanghai University, 200444 Shanghai, China*

² *Departamento de Química-Física, UPV-EHU, Apdo 644, 48080 Bilbao, Spain*

³ *Department of Physics, The Chinese University of Hong Kong, Shatin, New Territories, Hong Kong and*

⁴ *Department of Physics, Zhejiang University, Hangzhou 310027, China*

Motivated by the realization of the Dirac point (DP) with a double-cone structure for optical field in the negative-zero-positive index metamaterial (NZPIM), the reflection, transmission, and Goos-Hänchen (GH) shifts inside the NZPIM slab are investigated. Due to the linear Dirac dispersion, the transmission as the function of the frequency has a gap, thus the correspond reflection has a frequency or wavelength window for the perfect reflection, which is similar to the Bragg reflection in the one-dimensional photonic crystals. Near the DP, the associated GH shifts in the transmission and reflection can be changed from positive to negative with increasing the wavelength. These negative and positive shifts can also be enhanced by transmission resonances, when the frequency is far from that at the DP. All these phenomena will lead to some potential applications in the integrated optics and optical devices.

PACS numbers: 42.25.Gy, 42.25.Bs, 78.20.Ci

I. INTRODUCTION

It is well known that a light beam totally reflected from an interface between two dielectric media undergoes lateral shift from the position predicted by geometrical optics [1]. This phenomenon was referred to as the Goos-Hänchen (GH) effect [2] and was theoretically explained firstly by Artmann in 1948 [3]. Up till now, the investigations of the GH shifts have been extended to frustrated total internal reflection (FTIR) [4, 5, 6], attenuated total reflection (ATR) [7, 8], partial reflection [9, 10, 11, 12], and other areas of physics [2], such as quantum mechanics [13], acoustics [14], neutron physics [15], spintronics [16], atom optics [17] and graphene [18].

Graphene has become a subject of intense interest [19, 20] since the graphitic sheet of one-atom thickness has been experimentally realized by A. K. Geim *et al.* in 2004 [21]. The valence electron dynamics in such a truly two-dimensional (2D) material is governed by a massless Dirac equation. So graphene exhibits many unique electronic properties [19], including Klein tunneling [22]. On the other hand, the Dirac point (DP) in photonic crystals (PCs) for the Bloch states [23, 24, 25, 26] is found from the similarity of the photonic bands of the 2D PCs with the electronic bands of solids. Several novel optical transport properties near the DP have been shown in [24, 25, 26], such as conical diffraction [24], a “pseudodiffusive” scaling [25], and the photon’s Zitterbewegung [26]. Very recently, Wang *et al.* [27, 28] realized the DP with a double-cone structure for optical field in the negative-zero-positive index metamaterial (NZPIM),

and further the pseudodiffusive property [27] and Zitterbewegung effect [28] near the DP inside such optically homogenous media.

The main purpose of this paper is to investigate the transmission gap, Bragg-like reflection, and GH shifts near the DP inside a NZPIM slab. Due to the linear Dirac dispersion, the transmission has the frequency or wavelength stopping-band, thus the corresponding reflection has a frequency or wavelength window for perfect reflection, which is analogous to Bragg-like reflection in monolayer graphene barrier [29]. This so-called Bragg-like reflection in such a simple NZPIM slab is quite different from that in the 1D PCs (for instance, a stack of Bragg mirrors), resulting from the destructive and constructive interferences. More interestingly, the associated GH shifts in the reflection and transmission can be changed from positive to negative with increasing the wavelength near the DP. Also these negative and positive shifts can be enhanced by transmission resonances, when the frequency is far from that at the DP. All these phenomena will lead to some potential applications in the integrated optics and optical devices, such as frequency or wavelength filters and frequency-dependent spatial modulator.

II. MODEL

For simplicity, we consider a TE-polarized light beam with angular frequency ω and incidence angle θ_0 upon the NZPIM slab in the vacuum, as shown in Fig. 1, the dispersion of the NZPIM has a linear dispersion [27]

$$k(\omega) = (\omega - \omega_D)/v_D, \quad (1)$$

with group velocity $v_D = (d\omega/dk)|_{\omega=\omega_D}$, ω_D is the frequency of the DP (corresponding wavelength is $\lambda_D =$

*Email address: xchen@shu.edu.cn

†Email address: sxwlg@yahoo.com.cn

‡Email address: cfli@shu.edu.cn

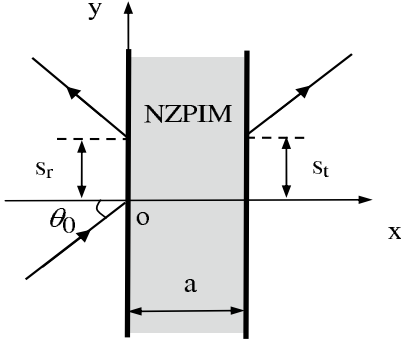


FIG. 1: Schematic diagram of the reflection and transmission inside the NZPIM slab configuration, where s_r and s_t denotes the GH shifts for the reflected and transmitted light beams, respectively.

$2\pi c/\omega_D$), where two bands touch each other forming a double-cone structure. Near the DP, the light transport obeys the massless Dirac equation as follows:

$$\begin{bmatrix} 0 & -i(\frac{\partial}{\partial x} - i\frac{\partial}{\partial y}) \\ -i(\frac{\partial}{\partial x} + i\frac{\partial}{\partial y}) & 0 \end{bmatrix} \Psi = \left(\frac{\omega - \omega_D}{v_D} \right) \Psi, \quad (2)$$

where $\Psi = \begin{pmatrix} E_{z1}(x, y, \omega) \\ E_{z2}(x, y, \omega) \end{pmatrix}$ are the eigenfunctions of the electric fields with the same $k(\omega)$. It is noted that the condition for realization of the DP in the homogenous optical medium is the index varying from negative to zero and then to positive with frequency [27], which is called as NZPIM. For simplicity, we take the Drude model as the parameters for both the relative permittivity and permeability of the NZPIM [27, 28]:

$$\varepsilon_1(\omega) = 1 - \omega_{ep}^2/(\omega^2 + i\gamma_e\omega), \quad (3)$$

$$\mu_1(\omega) = 1 - \omega_{mp}^2/(\omega^2 + i\gamma_m\omega), \quad (4)$$

where ω_{ep}^2 and ω_{mp}^2 are the electronic and magnetic plasma frequencies, and γ_e and γ_m are the damping rates relating to the absorption of the material. Here we can assume $\gamma_e = \gamma_m = \gamma \ll \omega_{ep}^2, \omega_{mp}^2$. It is important that when $\omega_{ep} = \omega_{mp} = \omega_D$ and $\gamma = 0$ (no loss), then both $\varepsilon_1(\omega_D)$ and $\mu_1(\omega_D)$ may be zero simultaneously. In this case, we find $k(\omega_D) \approx 0$ and $v_D \simeq c/2$, where c is the light speed in vacuum [28]. In what follows we will discuss the reflection, transmission, and the associated GH shifts near the DP in NZPIM slab.

III. REFLECTION AND TRANSMISSION

In this section, we will firstly investigate the properties of the reflection and transmission. Assuming the incident plane wave, $E_z^{in}(x, y) = \exp[i(k_x x + k_y y)]$, where $k_x = k_0 \cos \theta_0$, $k_y = k_0 \sin \theta_0$, $k_0 = \omega/c$ is the wave vector

in vacuum, the reflected and transmitted plane waves can be expressed by $E_z^{ref}(x, y) = r \exp[i(-k_x x + k_y y)]$ and $E_z^{tr}(x, y) = t \exp\{i[-k_x(x - a) + k_y y]\}$, where the reflection coefficient r is

$$r = \frac{\exp(i\pi/2)}{4g^2} \left(\frac{\mu_0 k_{1x}}{\mu_1 k_x} - \frac{\mu_1 k_x}{\mu_0 k_{1x}} \right) \times \left[\sin 2k_{1x}a + i \left(\frac{\mu_1 k_x}{\mu_0 k_{1x}} + \frac{\mu_0 k_{1x}}{\mu_1 k_x} \right) \sin^2 k_{1x}a \right], \quad (5)$$

and the transmission coefficient is $t = e^{i\phi}/g$ with the following complex number,

$$ge^{i\phi} = \cos k_{1x}a + \frac{i}{2} \left(\frac{\mu_1 k_x}{\mu_0 k_{1x}} + \frac{\mu_0 k_{1x}}{\mu_1 k_x} \right) \sin k_{1x}a,$$

with $k_{1x} = \sqrt{k_1^2 - k_y^2}$ and $k_1 = (\omega - \omega_D)/v_D$ near the DP. It is clear that the wave vector k_{1x} depends on the different frequencies ω and parallel wave vector k_y , which will resulting the unique properties of reflection and transmission in two cases of $\omega > \omega_D$ and $\omega < \omega_D$.

Case 1: $\omega > \omega_D$. The reflection probability R can be given by Eq. (5),

$$R \equiv |r|^2 = \frac{1}{4g^2} \left(\frac{\mu_0 k_{1x}}{\mu_1 k_x} - \frac{\mu_1 k_x}{\mu_0 k_{1x}} \right)^2 \sin^2 k_{1x}a, \quad (6)$$

and the transmission probability $T = 1 - R$ is also given by $T \equiv |t|^2 = 1/g^2$. Under resonance conditions, $k_{1x}a = N\pi$, ($N = 0, 1, \dots$), the reflection probability R_{min} reaches the zero and the transmission probability T_{max} is equal to 1. Otherwise, at the anti-resonances, $k_{1x}a = (N + 1/2)\pi$, ($N = 0, 1, \dots$) the reflection probability R tends to

$$R_{max} = \left(\frac{\mu_0 k_{1x}}{\mu_1 k_x} + \frac{\mu_1 k_x}{\mu_0 k_{1x}} \right) / \left(\frac{\mu_0 k_{1x}}{\mu_1 k_x} - \frac{\mu_1 k_x}{\mu_0 k_{1x}} \right), \quad (7)$$

and the corresponding transmission probability T_{min} is equal to

$$T_{min} = 4 / \left(\frac{\mu_0 k_{1x}}{\mu_1 k_x} + \frac{\mu_1 k_x}{\mu_0 k_{1x}} \right)^2, \quad (8)$$

However, we emphasize here that the reflection and transmission can be divided into evanescent and propagating modes, taking the influence of the incidence angle θ_0 into account. The propagation of the light beam inside the NZPIM slab can be evanescent when $\theta_0 > \theta_c$, where the critical angle for total reflection can be defined as

$$\theta_c = \sin^{-1} \left[2 \left(1 - \frac{\omega_D}{\omega} \right) \right], \quad (9)$$

with the necessary condition $\omega_D < \omega < 2\omega_D$. In this case, the transmission and reflection probabilities damped exponentially in the following form:

$$T \approx \frac{e^{-2\kappa a}}{1 + \frac{1}{4} \left(\frac{\mu_1 k_x}{\mu_0 k_{1x}} + \frac{\mu_0 k_{1x}}{\mu_1 k_x} \right)}, \quad (10)$$

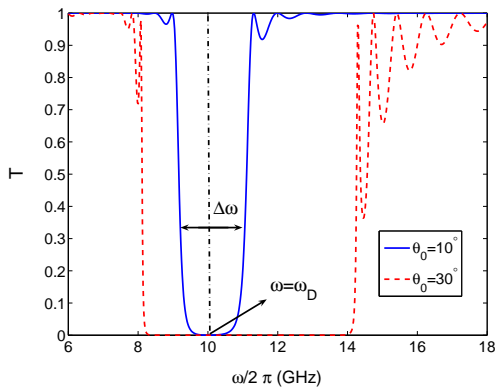


FIG. 2: (Color online) The transmission gap as the function of the frequency ω , where $a = 100$ mm, and $\omega_D = 10 \times 2\pi$ GHz. Solid and dashed curves correspond to $\theta_0 = 10^\circ$ and $\theta_0 = 30^\circ$.

and

$$R \approx 1 - \frac{e^{-2\kappa a}}{1 + \frac{1}{4} \left(\frac{\mu_1 k_x}{\mu_0 k_{1x}} + \frac{\mu_0 k_{1x}}{\mu_1 k_x} \right)}, \quad (11)$$

where $\kappa = [k_y^2 - k_1^2]^{1/2}$ is the decay constant. As a matter of fact, the light beam can transmit through the NZPIM slab in propagating mode at any incidence angles, when the critical angle θ_c is no longer valid for $\omega > 2\omega_D$.

Case 2: $\omega < \omega_D$. The reflection and transmission probability can be also damped exponentially when the incidence angle θ_0 is larger than the critical angle,

$$\theta'_c = \sin^{-1} \left[2 \left(\frac{\omega_D}{\omega} - 1 \right) \right], \quad (12)$$

with the necessary condition $\frac{2}{3}\omega_D < \omega < \omega_D$. On the contrary, the reflection and transmission probabilities will oscillate periodically on the thickness a of the slab, as mentioned *Case I*. In this case, the refractive index, defined as $n_1 = -\sqrt{\varepsilon_1 \mu_1}$, should be negative, which will lead to the negative GH shifts, as discussed later.

Based on the mentioned-above properties of the reflection and transmission in these two cases, the transmission as the function of frequency ω has a gap, as shown in Fig. 2, where $a = 100$ mm, and $\omega_D = 10 \times 2\pi$ GHz. Solid and dashed curves correspond to $\theta_0 = 10^\circ$ and $\theta_0 = 30^\circ$. Similarly, the transmission also has a stopping-band for the wavelength, since $\lambda = 2\pi\omega/c$. Since $k_{1x}^2 = (\omega - \omega_D)^2/v_D^2 - k_y^2 < 0$, the frequency region of the transmission gap in Fig. 2 is given by $\omega_D - k_y v_D < \omega < \omega_D + k_y v_D$, which leads to the width of transmission gap as follows,

$$\Delta\omega = 2k_y v_D. \quad (13)$$

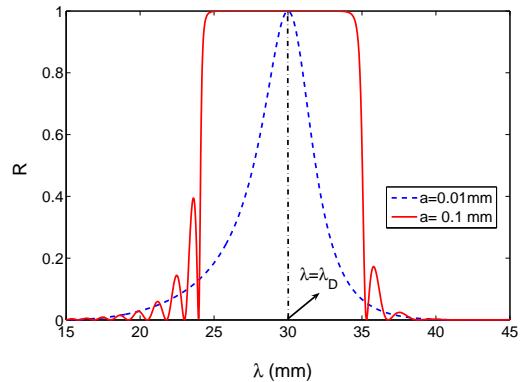


FIG. 3: (Color online) The reflection probability R as the function of the wavelength λ , where $\theta_0 = 20^\circ$, and other parameters are the same as in Fig. 2. Solid and dashed curves correspond to $a = 100$ mm and $a = 10$ mm.

This means $\Delta\omega/\omega = \sin \theta_0$ with the help of $v_D \simeq c/2$. It is further shown that the transmission gap with the center $\omega = \omega_D$ becomes narrower with the decrease of the incidence angle, and even vanishes at normal incidence. This transmission gap, which is analogous to that in single graphene barrier [29], is due to the evanescent waves in two cases of $\omega > \omega_D$ and $\omega < \omega_D$. Furthermore, the tunable transmission gap can be further understood by the dependence of the critical angle on the frequency, ω .

Fig. 3 indicates the dependence of corresponding reflection probability R on the wavelength $\lambda = 2\pi\omega/c$, where $\theta_0 = 20^\circ$, and other parameters are the same as in Fig. 2. Solid and dashed curves correspond to $a = 100$ mm and $a = 10$ mm. It is interesting that the light beam can be perfectly reflected by such single NZPIM slab at some range of the wavelength. As indicated in Fig. 3, the wavelength window for perfect reflection will become narrower with the increase of the width of slab, caused by the decay factor $\exp(-2\kappa a)$ in Eqs. (10) and (11). It is clearly seen from Fig. 2 that the reflection also has a similar frequency window for the perfect reflection, since $R = 1 - T$. These frequency or wavelength passing-band in reflected discussed here is similar to but different from the Bragg reflection in the 1D PCs. This so-called Bragg-like reflection discussed here is exactly due to the linear Dirac dispersion described by Eq. (1), which results in the evanescent waves in two cases of $\omega > \omega_D$ and $\omega < \omega_D$, corresponding to the two eigenfunctions of electric fields with the same $k(\omega)$. In a word, the Bragg-like reflection will provide alternative way to realize the frequency or wavelength filters with more design flexibility and miniaturization.

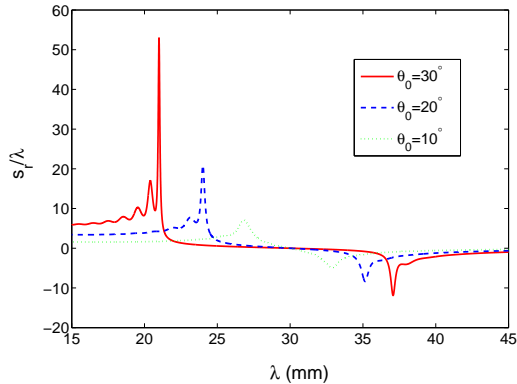


FIG. 4: (Color online) The GH shifts as the function of the wavelength, λ , where $a = 100$ mm, and other parameters are the same as in Fig. 2. Solid, dashed and dotted curves correspond to $\theta_0 = 30^\circ$, $\theta_0 = 20^\circ$, and $\theta_0 = 10^\circ$.

IV. GOOS-HÄNCHEN SHIFTS

Now, we have a look at the GH shifts in the reflection and transmission inside the single NZPIM slab. When a well-collimated light beam with the central incidence angle θ_0 is considered, the GH shifts in reflection and transmission, according to Artman's stationary phase method [3], can be defined as

$$s_{r,t} = -\frac{\partial \phi_{r,t}}{\partial k_y} \Big|_{\theta=\theta_0}, \quad (14)$$

where $k_y = k_0 \sin \theta$, θ represents the incidence angle of the plane wave component under consideration, $\phi_r = \phi + \pi/2$ and $\phi_t = \phi$ are the phase shifts of the reflected and transmitted light beams, respectively. Clearly, the GH shift in transmission is equal to that in reflection inside such symmetric slab configuration, because the values of the derivation of the phase shifts with respect to k_y are the same. Fig. 4 shows that the GH shifts can be positive and negative, where $a = 100$ mm, and other parameters are the same as in Fig. 2. Solid, dashed and dotted curves correspond to $\theta_0 = 30^\circ$, $\theta_0 = 20^\circ$, and $\theta_0 = 10^\circ$. It is shown that the GH shifts can be positive for $\lambda < \lambda_D$, while they can be negative for $\lambda > \lambda_D$. More interestingly, the GH shifts near the DP can change from positive to negative with the increase (decrease) of the wavelength (frequency).

Fig. 5 also shows the dependence of the GH shifts on the incident angle θ_0 , where $a = 100$ mm, and other parameters are the same as in Fig. 2. Solid, dashed, dotted and dot-dashed curves correspond to $\omega = 13 \times 2\pi$ GHz, $\omega = 11 \times 2\pi$ GHz, $\omega = 9 \times 2\pi$ GHz, and $\omega = 8 \times 2\pi$ GHz. It is reasonable that the GH shifts can be negative in the

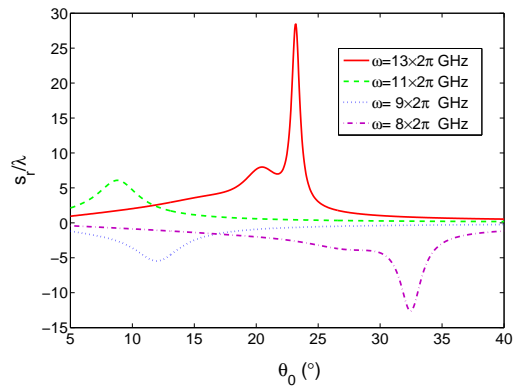


FIG. 5: (Color online) The GH shifts as the function of incidence angle θ_0 , where $a = 100$ mm, and other parameters are the same as in Fig. 2. Solid, dashed, dotted and dot-dashed curves correspond to $\omega = 13 \times 2\pi$ GHz, $\omega = 11 \times 2\pi$ GHz, $\omega = 9 \times 2\pi$ GHz, and $\omega = 8 \times 2\pi$ GHz.

case of $\omega < \omega_D$, where the refractive index $n_1 = -\sqrt{\varepsilon_1 \mu_1}$ is negative, while the GH shifts are positive in the case of $\omega > \omega_D$, where the refractive index $n_1 = \sqrt{\varepsilon_1 \mu_1}$ is positive. In addition, it is also shown that the GH shifts near the DP have only the order of wavelength due to the evanescent waves. The smallness of the GH shifts are similar to those in total reflection or FTIR structure. However, when the frequency is far from that at the DP, the incidence angle will be less than the critical angle, or there is no critical angle as discussed above. Thus, the negative and positive GH shifts can also be enhanced by the transmission resonances, as shown in Figs. 4 and 5. In addition, the GH shifts also depends on the width a of the slab. It can be predicted from Ref. [6] that the negative and positive GH shifts in the evanescent case will saturate to a constant with increasing the slab's width, when the incidence angle is larger than the critical angle. In a word, these negative and positive GH shifts are applicable to realize the frequency or wavelength filters in spatial domain, and frequency-dependent spatial modulator.

V. CONCLUSION

In conclusion, we have investigated the transmission gap, Bragg-like reflection, and the associated GH shifts inside the NZPIM slab. It is found that the transmission has a frequency stopping-band, thus the corresponding reflection has a frequency or wavelength window for the perfect reflection. This so-called Bragg-like reflection, resulting from the linear Dirac dispersion of NZPIM, is similar to but different from the Bragg reflection in the 1D PCs. In addition, the GH shifts near the DP can be changed from positive to negative with increasing wavelength, based on the unique properties of the reflection and transmissions. These negative and positive shifts can

also be enhanced by transmission resonances, when the frequency is far from that at the DP, ω_D . With the experimental realization of the NZPIM [30], we hope these phenomena will lead to some applications in the integrated optics and optical devices.

Acknowledgements

This work is supported by the National Natural Science Foundation of China (Grants No. 60806041, No.

10604047, and No. 60877055), the Shanghai Rising-Star Program (Grants No. 08QA14030), the Science and Technology Commission of Shanghai Municipal (Grants No. 08JC14097), the Shanghai Educational Development Foundation (Grants No. 2007CG52), and the Shanghai Leading Academic Discipline Program (Grants No. S30105). X. C. is also supported by Juan de la Cierva Programme of Spanish MICINN. L.-G. W. would like to thank the supports from CUHK 2060360 and RGC 403609.

-
- [1] F. Goos and H. Hänchen, *Ann. Phys.* **1**, 333 (1947); **5**, 251 (1949).
- [2] H. K. V. Lotsch, *Optik (Stuttgart)* **32**, 116 (1970); **32**, 189 (1970); **32**, 299 (1971); **32**, 553 (1971).
- [3] K. V. Artmann, *Ann. Phys. (Leipzig)* **2**, 87 (1948).
- [4] A. K. Ghatak, M. R. Shenoy, I. C. Goyal, and K. Thyagarajan, *Opt. Commun.* **56**, 313 (1986).
- [5] A. Haibel, G. Nimtz, and A. A. Stahlhofen, *Phys. Rev. E* **63**, 047601 (2001).
- [6] X. Chen, C.-F. Li, R.-R. Wei, Y. Zhang, *Phys. Rev. A* **80**, 015803 (2009).
- [7] X. Yin, L. Hesselink, Z. Liu, N. Fang, and X. Zhang, *Appl. Phys. Lett.* **85**, 372 (2004).
- [8] F. Pillon, H. Gilles, S. Girard, M. Laroche, R. Kaiser, and A. Gazibegovic, *J. Opt. Soc. Am. B* **22**, 1290 (2005).
- [9] C. W. Hsue and T. Tamir, *J. Opt. Soc. Am. A* **2**, 978 (1985).
- [10] R. P. Riesz and R. Simon, *J. Opt. Soc. Am. A* **2**, 1809 (1985).
- [11] C.-F. Li, *Phys. Rev. Lett.* **91**, 133903 (2003).
- [12] D. Müller, D. Tharanga, A. A. Stahlhofen, and G. Nimtz, *Europhys. Lett.* **73**, (2006) 526.
- [13] R.-H. Renard, *J. Opt. Soc. Am.* **54**, 1190 (1964).
- [14] R. Briers, O. Leroy, and G. Shkerdinb, *J. Acoust. Soc. Am.* **108**, 1624 (2000).
- [15] V.K. Ignatovich, *Phys. Lett. A* **322**, 36 (2004).
- [16] X. Chen, C.-F. Li, and Y. Ban, *Phys. Rev. B* **77**, 073307 (2008).
- [17] J.-H. Huang, Z.-L. Duan, H.-Y. Ling, and W.-P. Zhang, *Phys. Rev. A* **77**, 063608 (2008).
- [18] C. W. J. Beenakker, R. A. Sepkhanov, A. R. Akhmerov, and J. Tworzydło, *Phys. Rev. Lett.* **102**, 146804 (2009).
- [19] A. H. Castro Neto, F. Guinea, N. M. R. Peres, K. S. Novoselov and A. K. Geim, *Rev. Mod. Phys.* **81**, 1 (2009).
- [20] C. W. Beenakker, *Rev. Mod. Phys.* **80**, 1337 (2008).
- [21] K. S. Novoselov, A. K. Geim, S. V. Morozov, D. Jiang, Y. Zhang, S. V. Dubonos, I. V. Grigorieva, and A. A. Firsov, *Science* **306**, 666 (2004).
- [22] M. I. Katsnelson, K. S. Novoselov, and A. K. Geim, *Nat. Phys.* **2**, 620 (2006).
- [23] F. D. M. Haldane and S. Raghu, *Phys. Rev. Lett.* **100**, 013904 (2008).
- [24] O. Peleg, G. Bartal, B. Freedman, O. Manela, M. Segev, and D. N. Christodoulides, *Phys. Rev. Lett.* **98**, 103901 (2007).
- [25] R. A. Sepkhanov, Y. B. Bazaliy, and C. W. J. Beenakker, *Phys. Rev. A* **75**, 063813 (2007).
- [26] X. Zhang, *Phys. Rev. Lett.* **100**, 113903 (2008).
- [27] L.-G. Wang, Z.-G. Wang, J.-X. Zhang, and S.-Y. Zhu, *Opt. Lett.* **34**, 1510 (2009).
- [28] L.-G. Wang, Z.-G. Wang, and S.-Y. Zhu, *EPL* **86**, 47008 (2009).
- [29] X. Chen and J.-W. Tao, *Appl. Phys. Lett.* **94**, 262102 (2009).
- [30] L.-F. Zhang, G. Houzet, E. Lheurette, D. Lippens, M. Chaubet, and X.-P. Zhao, *J. Appl. Phys.* **103**, 084312 (2008).